Preprints of the 19th World Congress
The International Federation of Automatic Control
Cape Town, South Africa. August 24-29, 2014

Design and Modelling of a Quadrotor Helicopter with Variable Pitch Rotors for Aggressive Manoeuvres ⋆

Arnold Pretorius * **Edward Boje** **

* *Electrical Engineering Department, University of Cape Town, Cape Town, South Africa (e-mail: prtarn001@myuct.ac.za)*
** *Electrical Engineering Department, University of Cape Town, Cape Town, South Africa (e-mail: edward.boje@uct.ac.za)*

Abstract: This article presents the design of a low inertia, variable pitch quadrotor helicopter intended to investigate control problems associated with aggressive manoeuvres. In this paper a rotor pitch controlled quadrotor is designed and modelled to address performance limiting issues associated with conventional speed controlled quadrotors. The helicopter is designed to minimise the rotational inertia and maximise the vehicle bandwidth. Simple design and control measures are used to linearise the body attitude dynamics during all operating regions, aiding in complex acrobatic flight. The decoupled high performance capabilities are demonstrated by simulating a controlled 180° cross-axis roll.

Keywords: Quadrotor, Helicopter, Variable Pitch, UAV, Aerospace, Quaternion, Modelling.

1. INTRODUCTION

Quadrotor helicopters have recently received interest from hobbyists and research groups. In terms of their inherent control challenges the appeal of a four-bladed drone comes from its simple dynamic model compared to the more complex model of a conventional helicopter system.

The control challenge for UAVs (Unmanned Aerial Vehicles) is now focused on performing aggressive manoeuvres autonomously. Several groups have already succeeded in achieving fairly acrobatic flight regimes on physical quadrotors, see Cutler and How (2012) and Hoffmann et al. (2009). Generic control schemes such as Proportional-Derivative (PD) and Proportional-Integral (PI) controllers are commonly used to achieve satisfactory performance, but the result is that the quasi-decoupled attitude models only hold when actuated over a single degree of freedom and cannot handle aggressive cross-axis flight paths. Additionally, the vehicle mass moment of inertia plays a significant part in the system's bandwidth as the rotation dynamics inherently dictate the transverse motion of the quadrotor.

With the fairly recent introduction of variable pitch quadrotors, quadrotors can now do impressive manoeuvres without being restricted by the bandwidth limiting inertia of the motor-rotor pair (Cutler et al. (2012)). The pitch actuation of the rotor blades addresses the issue of the relatively slow motor time constant for acrobatic flight but does not alleviate the large mass moment of inertia caused by having four motors on the outside of the vehicle frame. This paper seeks to remedy the latter issues by the development of a novel variable pitch quadrotor with low inertia, shown in Fig. 1, designed for performing high angle of attack manoeuvres. The design uses two centrally located motors, spinning at the same speed in opposite directions, to drive each rotor pair at matched speeds via torque shafts. The thrust of each rotor blade is controlled by changing the blade pitch and this allows for high bandwidth thrust vectoring. The quadrotor is also designed to minimise the mass and rotational inertia of the vehicle and to remove attitude coupling from centrifugal and gyroscopic effects. The resulting quadrotor has a large thrust to weight ratio, low inertia, close to linear attitude dynamics, and is capable of fast acrobatic flight.

The structure of the paper is as follows: In Section 2 the full quadrotor model is derived, highlighting the key differences exhibited by the blade pitch actuation when compared to speed control. A preliminary analysis of the attitude dynamics is also presented to identify the problems with standard quadrotor models. Section 3 outlines the mechanical design based on the findings in Section 2,

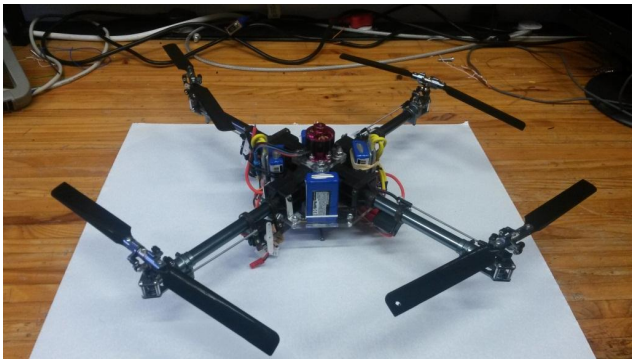

Fig. 1. Fully Assembled Variable Pitch Quadrotor Prototype

⋆ Financial support of the National Research Foundation and the University of Cape Town is gratefully acknowledged.

briefly presents the electronics used and gives a breakdown of the helicopter parameters. Section 4 shows a simulation of the quadrotor performing a 180° roll using a proportional quaternion-based state variable feedback controller. Section 5 concludes the paper and gives a brief discussion on future work.

2. MODELLING OF THE QUADROTOR

2.1 Co-ordinate Frames

The quadrotor orientation and position are described using the body-frame, in which the forces and torques are developed, and the inertial-frame, in which gravity acts and the quadrotor flies. The body-frame axes, described using a subscript 'b', are positioned on the quadrotor body with its origin coinciding with the vehicle centre of mass. As shown in Fig. 2, the body z-axis is chosen perpendicular

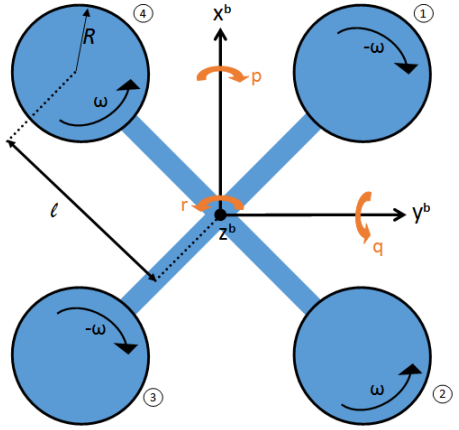

Fig. 2. Quadrotor with Body-Frame Axes Oriented in 'X'-Configuration with respective Rotational Velocities

to the quadrotor frame with the body x_by_b-plane rotated 45° from the conventional rotor-arm aligned plane. In this axis orientation, known as the 'x' configuration, the rotor pitch controlled quadrotor's aggressive manoeuvrability is maximised based on the allowable control authority, see Gupte et al. (2012). The body-frame velocity vector, $\mathbf{V}_b = [\dot{x}_b \quad \dot{y}_b \quad \dot{z}_b]^T$, describes the transverse motion of the quadrotor from a non-inertial viewpoint and the body-frame attitude rate vector, $\mathbf{\Omega}_b = [p \quad q \quad r]^T$ corresponds to the body roll, pitch and yaw rate respectively using the right hand rule notation.

The inertial-frame axes, denoted with subscript 'i' , are fixed at a grounded point which maps out a static 3-dimensional Cartesian plane. The location of the centre of mass of the helicopter in the inertial-frame is described by a Euclidean vector, $\mathbf{r}_i = [x_i \quad y_i \quad z_i]^T$, and the inertial-frame attitude is represented by the unit quaternion $\mathbf{q} = [q_o \; q_x \; q_y \; q_z]^T$, where q_o is a scalar and $[q_x \; q_y \; q_z]^T$ is a 3-element vector.

2.2 Generalised Acceleration Dynamics

The standard six degree of freedom model of a quadrotor is well known (Hoffmann et al. (2008), Stingu and Lewis (2009), and Kim et al. (2009)), with slight variations depending on the choice of rotation operator and to what extent external disturbances are accounted for.

The rectilinear dynamics of a rigid body UAV is described using point mass kinematics of the helicopter centre of mass. The absolute acceleration of the vehicle centre of mass, $\ddot{\mathbf{r}}_i$, is driven by the body-frame thrust, T_b, perpendicular to the body x_by_b-plane, and the gravitational acceleration, g_i, perpendicular to the inertial x_iy_i-plane. To describe the acceleration vector in the inertial-frame, the quaternion, $\mathbf{q}$, is used. The quaternion contains the inertial attitude information of the vehicle and can be used to map a body-frame vector, $\mathbf{v}_b$, to the inertial-frame vector, $\mathbf{v}_i$, by

$$\begin{bmatrix} 0 \\ \mathbf{v}_i \end{bmatrix} = \mathbf{q} \otimes \begin{bmatrix} 0 \\ \mathbf{v}_b \end{bmatrix} \otimes \mathbf{q}^*, \tag{1}$$

where $\otimes$ is the Kronecker product representing quaternion multiplication and $\mathbf{q}^* = [q_0 \quad -q_x \quad -q_y \quad -q_z]^T$ is the quaternion conjugate. For more information on quaternions, see Diebel (2006).

The resulting transverse acceleration vector can thus be described as

$$\begin{bmatrix} 0 \\ \ddot{\mathbf{r}}_i \end{bmatrix} = \frac{1}{m}\mathbf{q} \otimes \mathbf{T}_b \otimes \mathbf{q}^* + \mathbf{G}_i + \mathbf{D}_i, \tag{2}$$

where m is the UAV mass, $\mathbf{T}_b = [0 \quad 0 \quad 0 \quad T_b]^T$ is the resized body frame thrust vector, $\mathbf{G}_i = [0 \quad 0 \quad 0 \quad -g]^T$ is the inertial-frame gravitational acceleration vector and $\mathbf{D}_i = [0 \quad d_x \quad d_y \quad d_z]^T$ is the disturbance vector conveniently described in the inertial-frame.

Equation (2) can also be described by using a standard ψ-θ-ϕ rotation matrix. In this order the Euler angles, $\eta = [\phi \; \theta \; \psi]^T$, correspond sequentially to a yaw rotation, ψ, around the inertial z_i-axis, a pitch rotation, θ, about the inertial x_iy_i-plane, and a roll rotation, ϕ, about the body x_b-axis. The resuting acceleration vector is

$$\ddot{\mathbf{r}}_i = \frac{T_b}{m}\begin{bmatrix} \sin\phi\sin\psi + \cos\phi\sin\theta\cos\psi \\ \cos\phi\sin\theta\sin\psi - \sin\phi\cos\psi \\ \cos\theta\cos\phi \end{bmatrix} - \begin{bmatrix} 0 \\ 0 \\ g \end{bmatrix} + \begin{bmatrix} d_x \\ d_y \\ d_z \end{bmatrix}. \tag{3}$$

The rotational acceleration of the helicopter in the body frame, $\dot{\mathbf{\Omega}}_b$, is dependent on the centripetal forces, $\mathbf{\Omega}_b \times \mathbf{I}\mathbf{\Omega}_b$, gyroscopic moment, $\mathbf{\Gamma}_b$, and the torque generated by the rotors, $\mathbf{M}_b$. The generalised attitude dynamics can thus be described by

$$\mathbf{J}\dot{\mathbf{\Omega}}_b = \mathbf{M}_b - \mathbf{\Omega}_b \times \mathbf{J}\mathbf{\Omega}_b - \mathbf{\Gamma}_b + \mathbf{\Delta}_b, \tag{4}$$

where $\mathbf{J} \in \mathbb{R}^{3\times3}$ is a diagonal mass moment of inertia matrix and $\mathbf{\Delta}_b = [\delta_\phi \; \delta_\theta \; \delta_\psi]^T$ is the vector corresponding to external body-frame moment disturbances.

The generalised dynamics, shown in (2) and (4), describe any rigid-body six degree-of-freedom vehicle. In the case of a pitch controlled quadrotor, the thrust and torque, which make up the full control input vector of the vehicle, $\mathbf{U_c} = [T \quad \mathbf{M}_b{}^T]^T$, are functions of the commanded blade pitch, and not the rotor speeds and accelerations. In particular, the rotor angular velocities are held constant by speed controllers and are treated as static variables. This completely removes the motor dynamics from the thrust actuation. The rotor blade pitch is used to vary the thrust

and torque of each rotor individually and is only limited by the servo motor speed and blade stall angle.

2.3 Thrust and Torque Equations

Using blade element theory and momentum theory (Padfield (2007)), the thrust and torque for a rotor can be found. The thrust and torque of a two-bladed symmetrical propeller are functions of the air density, ρ, chord width c, rotor speed ω, effective angle of attack α, rotor inflow velocity ε, resultant air speed v_R, and respective lift and drag coefficients, C_{L_α}, C_{D_α} and C_{D_o}.

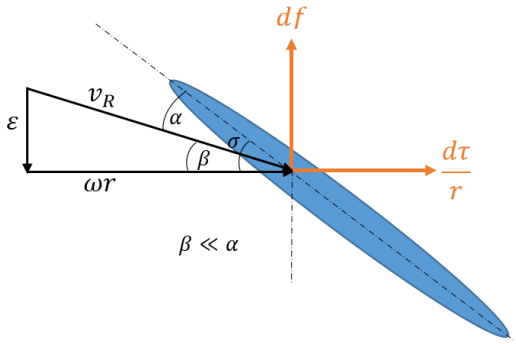

Fig. 3. Propeller Blade Element Velocity and Force Diagram

Using a small angle approximation for the inflow angle of $\beta = \frac{\varepsilon}{\omega r}$, shown in Fig. 3, and integrating along the blade length, the thrust for rotor $k \in \{1, 2, 3, 4\}$, can be written as

$$f_k = B_{L_\sigma}\sigma_k - B_{L_\varepsilon}\varepsilon_k, \tag{5}$$

where $B_{L_\sigma} = \frac{1}{3}\rho c C_{L_\alpha}\omega^2 R^3$, $B_{L_\varepsilon} = \frac{1}{2}\rho c C_{L_\alpha}\omega R^2$, and $\sigma_k = \alpha_k + \beta_k$ is the commanded blade angle. The normalised lift, $f_k(\sigma, \varepsilon)/f_k(\sigma, 0)$, is illustrated with respect to $\frac{\varepsilon}{\omega R}$ in Fig. 4, showing gain uncertainty as a result of inflow and commanded blade angle.

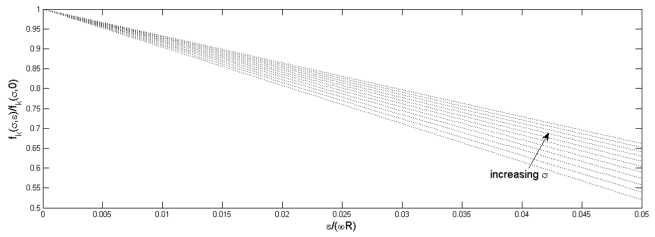

Fig. 4. Normalised Lift with Respect to Inflow Angle

Similarly, the torque magnitude for rotor k is approximately

$$|\tau_k| = B_{D_\sigma}\sigma_k^2 + B_{D_{\varepsilon,\sigma}}\varepsilon_k\sigma_k + B_{D_\varepsilon}\varepsilon_k^2, \tag{6}$$

where $B_{D_\sigma} = \frac{1}{4}\rho c R^4\omega^2 C_{D_\alpha}$, $B_{D_{\sigma,\varepsilon}} = \frac{1}{3}\rho c R^3\omega(C_{L_\alpha} - 2C_{D_\alpha})$, and $B_{D_\varepsilon} = \frac{1}{2}\rho c R^2(C_{L_\alpha} + C_{D_\alpha})$. A term, $\omega^2 C_{D_o}\frac{R^4}{4}$, has been omitted from the torque equation as it will be constant for each rotor and is therefore cancelled when summing all rotor moments. These results are in line with those of Bristeau et al. (2009) for symmetrical, uncambered propellers. Only the first terms in (5) and (6) are the result of control action.

2.4 Modelling the Control Action

From Fig. 4, the total force produced is a function of the physically commanded angle with gain uncertainty determined by the inflow velocity. The net thrust of the vehicle is the sum of each rotor thrust,

$$T = \sum_{k=1}^{4} f_k = B'_{L_\sigma}\sum_{k=1}^{4}\sigma_k, \tag{7}$$

where B'_{L_σ} has absorbed the uncertainty. Similarly, the total controllable torque around the z-axis is the sum of each rotor torque,

$$M_\psi = B'_{D_\sigma}\sum_{k=1}^{4}(-1)^{k+1}\sigma_k^2, \tag{8}$$

where the direction is governed by the right hand rule convention and the coefficient, B'_{D_σ}, has absorbed the uncertainty. Referring to Fig. 2, the commanded roll and pitch torques, around the body x_b- and y_b-axes respectively, are simply the torques generated by the differential rotor thrusts about the centre of mass,

$$\begin{bmatrix} M_\phi \\ M_\theta \end{bmatrix} = \begin{bmatrix} \frac{\ell}{\sqrt{2}}B'_{L_\sigma}(-\sigma_1 - \sigma_2 + \sigma_3 + \sigma_4) \\ \frac{\ell}{\sqrt{2}}B'_{L_\sigma}(\sigma_1 - \sigma_2 - \sigma_3 + \sigma_4) \end{bmatrix} \tag{9}$$

where $\frac{\ell}{\sqrt{2}}$ is the perpendicular torque arm. In order to decouple the control vector the following substitution is made,

$$\mathbf{U} = \begin{bmatrix} u_1 \\ u_2 \\ u_3 \\ u_4 \end{bmatrix} = \begin{bmatrix} \sigma_1 + \sigma_2 + \sigma_3 + \sigma_4 \\ -\sigma_1 - \sigma_2 + \sigma_3 + \sigma_4 \\ \sigma_1 - \sigma_2 - \sigma_3 + \sigma_4 \\ \sigma_1^2 - \sigma_2^2 + \sigma_3^2 - \sigma_4^2 \end{bmatrix}. \tag{10}$$

Equation (10) describes the usable input vector. Following this, the resulting decoupled control vector is

$$\mathbf{U}_c = \begin{bmatrix} T \\ M_\phi \\ M_\theta \\ M_\psi \end{bmatrix} = \begin{bmatrix} B'_{L_\sigma}u_1 \\ \frac{\ell}{\sqrt{2}}B'_{L_\sigma}u_2 \\ \frac{\ell}{\sqrt{2}}B'_{L_\sigma}u_3 \\ B'_{D_\sigma}u_4. \end{bmatrix}. \tag{11}$$

2.5 Mapping of the Input Vector

The controllable input vector introduced in (10) describes the four inputs as functions of the blade pitch angles, and is useful in establishing a decoupled multi-input-multi-output relationship. The inverse of this function, $\mathbf{\Xi} = \mathbf{f}^{-1}(\mathbf{U})$, allows calculation of physical pitch commands to each servo motor:

$$\mathbf{\Xi} = \begin{bmatrix} \sigma_1 \\ \sigma_2 \\ \sigma_3 \\ \sigma_4 \end{bmatrix} = \frac{1}{4u_1}\begin{bmatrix} 2u_4 - u_1u_2 + u_1u_3 + u_2u_3 + u_1^2 \\ -2u_4 - u_1u_2 - u_1u_3 - u_2u_3 + u_1^2 \\ 2u_4 + u_1u_2 - u_1u_3 + u_2u_3 + u_1^2 \\ -2u_4 + u_1u_3 + u_1u_2 - u_2u_3 + u_1^2 \end{bmatrix}. \tag{12}$$

It is important to note that this unique mapping contains a singularity at $u_1 = 0$ and places a strict constraint on the commanded acceleration in the body z direction. Interestingly, the quadrotor still has some controllability when in this free fall, such as the case when $u_1 = 2u_4 + u_2u_3 = 0$, resulting in

$$\begin{bmatrix}\sigma_1\\ \sigma_2\\ \sigma_3\\ \sigma_4\end{bmatrix} = \frac{1}{4}\begin{bmatrix}-u_2+u_3\\ -u_2-u_3\\ u_2-u_3\\ u_2+u_3\end{bmatrix}, \tag{13}$$

which allows for feather-like body rolling and pitching.

2.6 Preliminary Analysis of the Attitude Dynamics

Consider again the attitude behaviour developed in (4) of

$$\mathbf{J}\dot{\mathbf{\Omega}}_b = \mathbf{M}_b - \mathbf{\Omega}_b \times \mathbf{J}\mathbf{\Omega}_b - \mathbf{\Gamma}_b + \mathbf{\Delta}_b.$$

Given that the mass moment of inertia matrix is in the form of a 3x3 diagonal matrix, $\mathbf{J} = \texttt{diag}(J_{xx}, J_{yy}, J_{zz})$, the rotational dynamics can explicitly be written as

$$\mathbf{J}\dot{\mathbf{\Omega}}_b = \mathbf{M}_b - \begin{bmatrix}(J_{zz}-J_{yy})qr\\ (J_{xx}-J_{zz})pr\\ (J_{yy}-J_{xx})pq\end{bmatrix} - \mathbf{\Gamma}_b + \mathbf{\Delta}_b, \tag{14}$$

where $\mathbf{\Omega}_b = [p\ q\ r]^T$. Expanding the term for the gyroscopic moment,

$$\begin{aligned}\mathbf{\Gamma}_b =& J_r\mathbf{\Omega}_b \times \sum_{k=1}^{4}\omega_k + J_m\mathbf{\Omega}_b \times \sum_{t=1}^{2}\omega_{m_t}\\ =& \begin{bmatrix}q\\ -p\\ 0\end{bmatrix}(J_r(\omega_1+\omega_3-\omega_2-\omega_4) + J_m(\omega_{m_1}-\omega_{m_2}))\\ =& \begin{bmatrix}q\\ -p\\ 0\end{bmatrix}K(\omega_{m_1}-\omega_{m_2}),\end{aligned} \tag{15}$$

where ω_k is the angular velocity of rotor k, ω_{m_t} is the angular velocity of motor t, J_r and J_m are the rotor and motor's inertia respectively, G is the gear ratio from motor t to rotor k, and $K = J_m + \dfrac{2J_r}{G}$.

If the motor speeds are regulated such that $|\omega_{m_1}| = |\omega_{m_2}|$, the angular momentum and thus the gyroscopic moment will be zero for all time. With reference to (14), as the quadrotor is designed with $J_{xx} = J_{yy}$, there is no centripetal coupling around the z-axis. If $r = 0$, there is no coupling around the x- and y-axes. This constraint does not limit the fundamental motion of the vehicle as the inertial-frame thrust vector is completely independent of the body-frame yaw dynamics. Following these design and control measures, the simplified linear attitude dynamics are

$$\mathbf{J}\dot{\mathbf{\Omega}}_b = \mathbf{M}_b + \mathbf{\Delta}_b. \tag{16}$$

Equation (16) is linear for all operating regions and does not suffer from any coupling when actuating over more than one degree of freedom. The inertia values, J_{xx}, J_{yy} and J_{zz}, serve as open-loop gain attenuation in (16) and should be minimised for high bandwidth performance. The same applies for the mass in (2). If the differential motor velocity, $\triangle\omega_m = \omega_{m_1} - \omega_{m_2}$, is non zero and slowly time varying, this will result in small cross-axis damping,

$$\mathbf{\Gamma}_b = \begin{bmatrix}0 & K\triangle\omega_m & 0\\ -K\triangle\omega_m & 0 & \\ 0 & 0 & 0\end{bmatrix}\mathbf{\Omega}_b. \tag{17}$$

3. HARDWARE DEVELOPMENT

The quadrotor developed for this control project was made using readily available remote control helicopter parts and was designed with the following objectives:

- Rotational symmetry, $J_{xx} = J_{yy}$
- Minimise the mass, m and mass moment of inertia, $\mathbf{J}$
- Maximise the thrust to weight ratio $T_b : m$
- Motors coaxially placed rotating in opposite directions with equal rotational speed.

3.1 Mechanical Design

The motors, rotors and gearing were optimised to trade off mass and inertia with lift, power and endurance. In order to maintain symmetry around the body x_by_b-plane as well as keep the mass moment inertia at a minimum, the two motors were mounted co-axially, at the centre of the quadrotor frame as shown in Fig. 5. The pinions of the two motors each drive a pair of gears which transfer power to rotors via torque shafts. In this configuration,

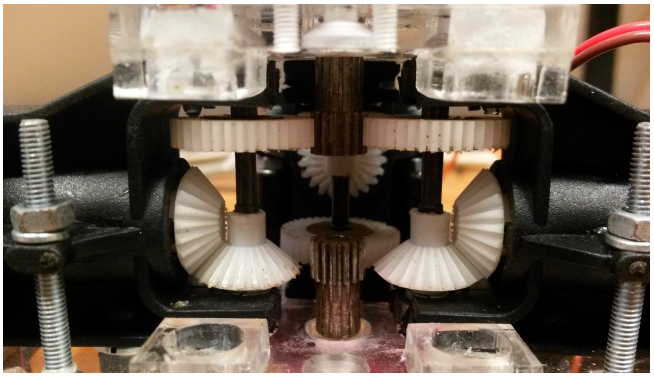

Fig. 5. Front View of Quadrotor Gearbox from the Perspective of a Removed Rotor Arm

shown in Fig. 2, motor 1 will drive one opposing pair of rotors and motor 2 will drive the other rotor pair in the other direction. Modified tail assemblies of a remote control helicopter are used as rotor arms with the torque shafts running inside the aluminium tubing as seen in Fig. 6. Servo motors, mounted on each rotor arm, are used to actuate the pitch motion on the tail rotors. Four batteries are placed symmetrically around the gearbox and are connected in parallel. Table 1 contains the detailed quadrotor specifications.

Table 1. Detailed UAV Specifications

Specification	Value
Mass, m (g)	870
Mass moment of inertia, J_{xx} (kg.mm^2)	2876
Mass moment of inertia, J_{yy} (kg.mm^2)	2855
Mass moment of inertia, J_{zz} (kg.mm^2)	5290
Blade Radius , R (mm)	136
Rotor Arm Length, ℓ (mm)	203
Coefficient of Lift, C_{L_α}	5.56
Coefficient of Drag, C_{D_α}	1.87
Operating Angular Velocity, ω (rad/s)	576
Thrust to Weight Ratio	3 : 1
Gear Ratio	2.67
Servo Motor Time Constant (s)	0.020

3.2 Electronic Hardware

The on-board electronics includes two electronic speed controllers (ESC), a 9 degree of freedom inertial measurement unit (IMU), a Wi-Fi communication module, and a microcontroller. Using the accelerometer and gyroscope readings from the IMU, a non-absolute estimate of the body-frame dynamics can be made. The inertial-frame position and attitude of the quadrotor is then given by fixed cameras set-up in a pre-defined space. Localisation is performed by detecting coloured balls attached to the quadrotor rotor arm ends and then using low-cost image processing to locate the vehicle centre of mass. Based on the dependence on a ground-based computer and the small size of the quadrotor, it was decided that all the low-level processing, inner loop angular rate feedback and overall control actuation is to be performed on a small on-board microcontroller and all the high-level, computationally taxing algorithms are to be executed on the ground-based computer. Table 2 shows the various components used.

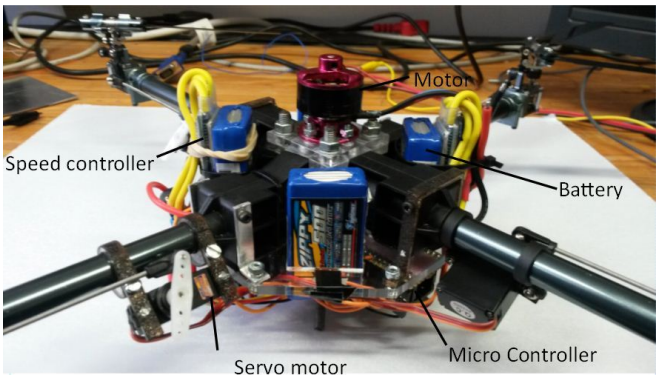

Fig. 6. View of Quadrotor with all Components on Board

Table 2. Breakdown of Physical Components

Component	Type	Quantity
Motor	250W, 1650 Kv/V	2
Speed Controller	20A/30A	2
Servo Motor	929mg, 60°/0.01s	4
Battery	500mAh 20/30C	4
Microcontroller	Teensy 3.0, 48Mhz	1
Wi-Fi Module	Roving Networks	1
Inertial Measurement Unit	MPU-9150, 9DoF	1
Central Platforms	ABS Plastic	N/A
Rotor Arms	Aluminium Tube	4

4. PRELIMINARY SIMULATIONS

To demonstrate the decoupled high-bandwidth potential of the designed quadrotor a controlled 180° cross-axis roll, requiring large signal actuation in the body-frame roll and pitch channels, was simulated in `Simulink`. For simplicity sake rectilinear control was neglected. The simulation model includes the inherent quadrotor limitations such as the propeller critical angle of attack, servo motor rate limits and approximated first order servo motor time constants, and makes use of the model and system parameters developed in the previous sections. The controller utilises proportional attitude state variable feedback (effectively PD controllers on the quaternion errors) based on the work of Michini (2009) and Song et al. (2006).The attitude state vector, $\mathbf{X_\eta}$, is made up of the decomposed body-frame quaternion error, $\mathbf{\Theta_b^e}$, and the body rate vector, $\mathbf{\Omega}_b$,

$$\mathbf{X_\eta} = \left[\mathbf{\Theta_b^e}^T \ \mathbf{\Omega}_b^T\right]^T = \left[q_x^e \ q_y^e \ q_z^e \ p \ q \ r\right]^T, \tag{18}$$

where $\mathbf{\Theta_b^e} = \left[q_x^e \ q_y^e \ q_z^e\right]^T$ is the vectorial part of the body-frame quaternion error, $\mathbf{q_b^e} = \mathbf{q_d^*} \otimes \mathbf{q} = \left[q_o^e \ q_x^e \ q_y^e \ q_z^e\right]^T$, $\mathbf{q}$ is the actual (measured) quaternion containing the inertial-frame pose, and $\mathbf{q_d}$ is the desired inertial-frame quaternion. The proportional state feedback controller is

$$\mathbf{U_\eta} = \left[u_2 \ u_3 \ u_4\right]^T = -\mathbf{K_p}\mathbf{\Theta_b^e} - \mathbf{K_d}\mathbf{\Omega}_b, \tag{19}$$

where $\mathbf{K_p}$ and $\mathbf{K_d}$ are 3x3 diagonal matrices implemented as shown in Fig. 10. For a step change in the desired quaternion, infinitely many attitude trajectories are possible and to resolve this, spatially continuous commands are used. In Fig. 10, the servo motor transfer function matrix, $\mathbf{N(s)} \in \mathbb{R}^{4\times4}$, and prefilter transfer function matrix, $\mathbf{P(s)} \in \mathbb{R}^{4\times4}$, are modelled with diagonal unity gain first order lag filters with a time constant of $T = 0.02s$,

$$\mathbf{P(s)} = \mathbf{N(s)} = \frac{1}{1+0.02s}\mathbf{I}, \tag{20}$$

where $\mathbf{I} \in \mathbb{R}^{4\times4}$ is the identity matrix, $\mathbf{M_{q\to\theta}}$ describes the mapping from the 4-element quaternion error, $\mathbf{q_b^e}$, to the 3-element purely vectorial quaternion error, $\mathbf{\Theta_b^e}$, and $\mathbf{f^{-1}}$, introduced in Section 2.5, maps the control action to the desired blade pitch angles.

The desired quaternion of $\mathbf{q_d} = \left[0 \ \frac{1}{\sqrt{2}} \ \frac{1}{\sqrt{2}} \ 0\right]^T$, corresponding to a 180° roll about rotor arm 1 in Fig. 2 or a ψ-θ-ϕ Euler setpoint of $\boldsymbol{\eta_d} = \left[\pi \ 0 \ -\frac{\pi}{2}\right]^T$, is applied at $t = 0.1s$ with all initial conditions (including the blade pitch angles) set to zero. The resulting time response and blade pitch angles are shown in Fig. 7 and Fig. 8 respectively. The behaviour of the quaternion error is shown in Fig. 9 and the chosen control parameters and physical limations are shown in Table 3. The controller gains in Table 3 are from the state variable errors to the mixed blade pitch angles in Equation (10) and do not include the aerodynamic coefficients in Equation (11). The quaternion errors, shown in Fig. 9, approach the desired zero error steady-state tensor of $(\mathbf{q_b^e})_{\mathbf{ss}} = [1 \ 0 \ 0 \ 0]^T$ and exhibit the same damped second order behaviour as the Euler angles in Fig. 7. The blade pitch angles in Fig. 8 quickly approach their saturation limits of $\sigma_{max} = 0.175(rad/s)$ during the first half of the manoeuvre followed by a braking motion before reaching a steady-state attitude at approximately 0.5 seconds.

Table 3. Control Parameters and Physical Limitation Values

Parameter	Value
Critical Angle of Attack (°)	10
Servo Motor Time Constant (s)	0.020
Servo Motor Rate Limit (rad/s)	10.47
Induced Velocity, ε_k (ms^{-1})	4.77
Position Controller, $\mathbf{K_p}$	**diag**(0.69,0.69, 0.81)
Velocity Controller, $\mathbf{K_d}$	**diag**(0.044, 0.044, 0.06)

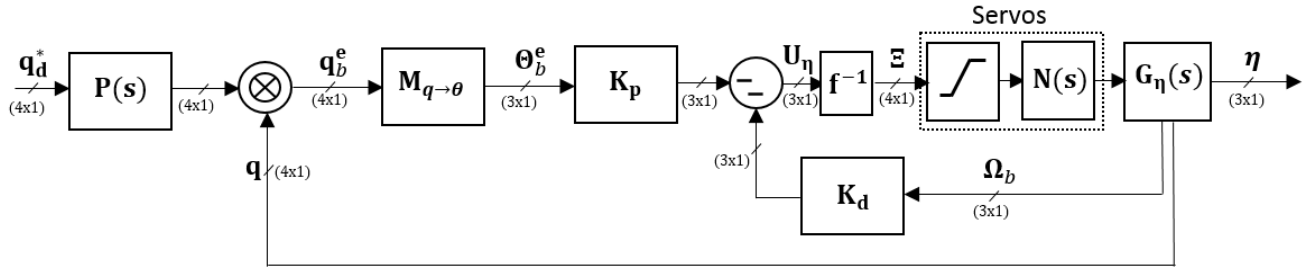

Fig. 10. System Block Diagram of Full Proportional Quaternion State Feedback Controller on Quadrotor Helicopter

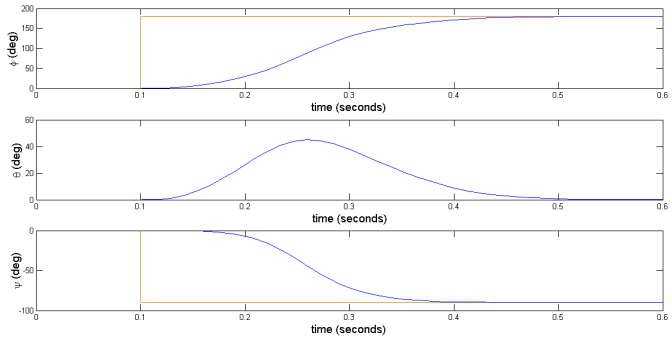

Fig. 7. Time Response of 180° Commanded Cross-Axis Roll

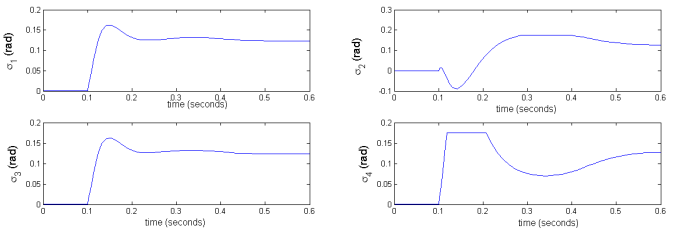

Fig. 8. Physical Blade Angles with 180° Commanded Cross-Axis Roll

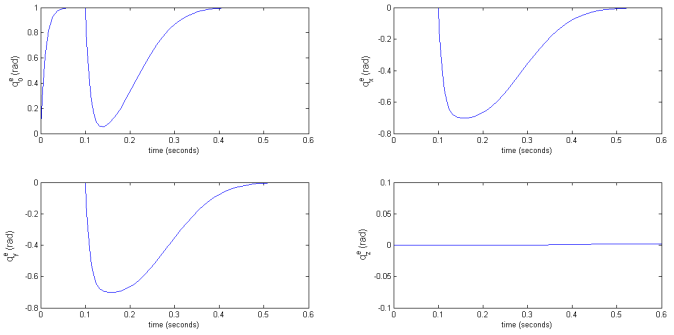

Fig. 9. Quaternion Error from 180° Commanded Cross-Axis Roll

5. DISCUSSION AND CONCLUSION

A novel design of a quadrotor helicopter to achieve an agile UAV with minimised attitude coupling and maximised control authority has been presented. The vehicle dynamics were modelled, using the blade pitch actuation as the control method, and physical design considerations were made to linearise the body-frame attitude dynamics. The mechanical design and hardware choices were briefly explained, based on the aforementioned objectives. Finally, a simple attitude controller was used to show the theoretical high angle of attack capabilities of the quadrotor in a simulation environment. Future work will include implementing the attitude controller on the constructed quadrotor, developing a robust controller for the transverse dynamics, and integrating the two controllers with a trajectory planning algorithm.

REFERENCES

Bristeau, P.J., Martin, P., Salaün, E., and Petit, N. (2009). The Role of Propeller Aerodynamics in the Model of a Quadrotor UAV. *European Control Conference*, 683–688.

Cutler, M. and How, J. (2012). Actuator Constrained Trajectory Generation and Control for Variable-Pitch Quadrotors. *AIAA Guidance, Navigation, and Control Conference*, 1–13.

Cutler, M., Ure, Michini, B., and How, J.P. (2012). Comparison of Fixed and Variable Pitch Actuators for Agile Quadrotors. *In AIAA Guidance, Navigation, and Control Conference (GNC)*, 1–17.

Diebel, J. (2006). Representing Attitude: Euler Angles, Unit Quaternions, and Rotation Vectors. *Matrix*.

Gupte, S., Conrad, J.M., and Mohandas, P. (2012). A Survey of Quadrotor Unmanned Aerial Vehicles. *Southeastcon, 2012 Proceedings of IEEE*.

Hoffmann, G., Waslander, S., and Tomlin, C. (2008). Quadrotor Helicopter Trajectory Tracking Control. *AIAA Guidance, Navigation and Control Conference and Exhibit*, 1–14.

Hoffmann, G., Waslander, S., and Tomlin, C. (2009). Aerodynamics and control of autonomous quadrotor helicopters in aggressive maneuvering. *2009 IEEE International Conference on Robotics and Automation*, 3277–3282.

Kim, J., Kang, M.S., and Park, S. (2009). Accurate Modeling and Robust Hovering Control for a Quadrotor VTOL Aircraft. *Journal of Intelligent and Robotic Systems*, 57(1-4), 9–26.

Michini, B. (2009). Modeling and Adaptive Control of Indoor Unmanned Aerial Vehicles. *Diss. Massachusetts Institute of Technology*.

Padfield, G.D. (2007). *Helicopter Flight Dynamics*. Blackwell Publishing Ltd, Oxford, UK.

Song, C., Kim, S.J., Kim, S.H., and Nam, H. (2006). Robust control of the missile attitude based on quaternion feedback. *Control Engineering Practice*, 14(7), 811–818.

Stingu, E. and Lewis, F. (2009). Design and implementation of a structured flight controller for a 6DoF quadrotor using quaternions. In *2009 17th Mediterranean Conference on Control and Automation*, 1233–1238. IEEE.